JACS
JOURNAL OF THE AMERICAN CHEMICAL SOCIETY

Article

pubs.acs.org/JACS

Conformational Analysis of Chiral Supramolecular Aggregates: Modeling the Subtle Difference between Hydrogen and Deuterium

Yoko Nakano,[†,‡] Albert J. Markvoort,[‡,§] Seda Cantekin,[†,‡] Ivo A. W. Filot,[‡] Huub M. M. ten Eikelder,[‡,§] E. W. Meijer,*[,†,‡] and Anja R. A. Palmans*[,†,‡]

[†]Laboratory of Macromolecular and Organic Chemistry, [‡]Institute for Complex Molecular Systems, and [§]Computational Biology Group, Eindhoven University of Technology, P.O. Box 513, 5600 MB Eindhoven, The Netherlands

Supporting Information

ABSTRACT: A detailed analysis of the conformational states of self-assembled, stereoselectively deuterated benzene-1,3,5-tricarboxamides ((*S*,*S*,*S*)-D-BTAs) reveals four different conformers for the supramolecular polymers. The relative amount of the conformers depends on the solvent structure and the temperature. With the help of a model, the thermodynamic parameters that characterize the different conformational states were quantified as well as the amount of the species that occur at different stages of the polymerization process. The results show that small changes in the stability between different types of conformers formed by (*S*,*S*,*S*)-D-BTAs—in the order of a few J mol^{-1}—arise from the combination of interactions between the solvent/supramolecular aggregate, temperature, and solvent structure. While the introduction of a deuterium label allows to sensitively probe the solvophobic effects in the supramolecular aggregation, a rationalization of the observed effects on a molecular level is not yet straightforward but is proposed to result from subtle effects in the vibrational enthalpy and entropy terms of the isotope effect.

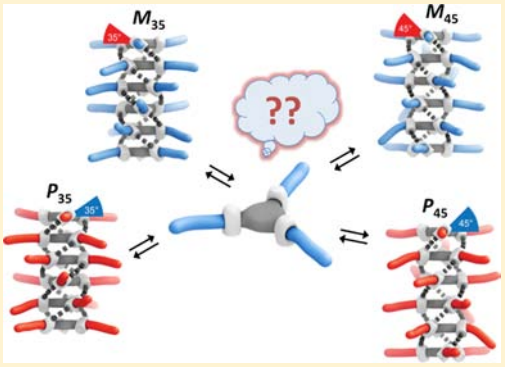

INTRODUCTION

Chirality resulting from isotope substitution is an intriguing research topic that continues to fascinate the scientific community.[1] In addition, changing one hydrogen (stereoselectively) for a deuterium results in profound differences in the conformational preferences of cyclic alkanes,[2] the helical bias in dynamic polymers,[3] and the stability of supramolecular complexes.[4] Likewise, isotope substitution is a powerful tool in the elucidation of reaction pathways in transition-metal- and enzyme-catalyzed (asymmetric) reactions.[5] The differences in zero-point energy between C−H and C−D bonds are often invoked to rationalize the origin of the observed deuterium isotope effects.[6] However, deuteration does not only change the length between C−H versus C−D bonds but also the physical properties of the molecules such as polarity, polarizability, and molecular volume.[7]

In a recent communication, we exchanged one hydrogen for a deuterium at the α-position of *N*,*N*′,*N*′′-trioctyl-benzene-1,3,5-tricarboxamides (BTAs) and found that this suffices to induce a preferred helical sense in the supramolecular aggregate (Figure 1A).[8] In addition, we reported that the self-assembly of these selectively deuterated BTAs (D-BTAs) is highly sensitive to the molecular structure of the alkane solvent applied.[9] Linear alkane solvents interact with the alkyl side chains of the helical columnar aggregates formed by D-BTAs, while branched solvents do not. This behavior results in the existence of two different conformations of the hydrogen-bonding amides having an angle θ of 35° or 45° with respect to the central benzene ring (Figure 1B). In addition, the presence of a chiral center biases one helical conformation, right-handed (*P*) or left-handed (*M*), over the other in the aggregates formed. As a result, at room temperature self-assembled (*S*,*S*,*S*)-D-BTA can

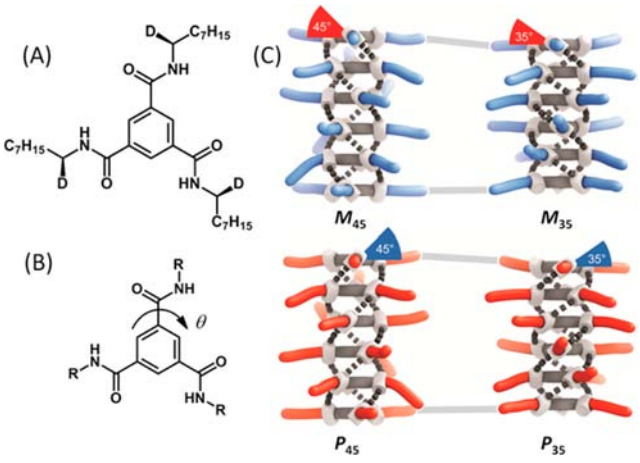

Figure 1. (A) Chemical structure of (*S*,*S*,*S*)-D-BTA. (B) Dihedral angle (θ) between the amide and the central benzene core. (C) Four distinct conformational states exist in BTA-based supramolecular polymers, differing in θ (45° and 35°) and helical sense (*P* or *M*).

Received: July 18, 2013
Published: October 7, 2013

   dx.doi.org/10.1021/ja4073645 | *J. Am. Chem. Soc.* 2013, 135, 16497−16506

be present in four different conformational states namely M_{45}, M_{35}, P_{35}, or P_{45} (Figure 1C). Circular dichroism (CD) spectroscopy allows to distinguish which conformer is most dominant by analyzing the shape (double Cotton effect: 35° conformer; single Cotton effect: 45° conformer), sign (positive Cotton effect: *P* helical sense, negative Cotton effect: *M* helical sense), and size of the CD spectra.[10]

In this work, we present a detailed conformational analysis of the self-assembly of (*S*,*S*,*S*)-D-BTAs as a function of solvent and temperature by combining experimental work and a theoretical analysis of the results. This approach leads to an in-depth understanding of the conformational changes that D-BTAs show as a response to solvent and temperature. We present a mathematical model that elucidates which different species are formed at the different stages of the supramolecular polymerization and how their relative stabilities depend on solvent and temperature. Finally, we rationalize the behavior of the D-BTA-based supramolecular polymers by analyzing their free energies as a function of temperature. The energies involved to switch from one conformational state to another are remarkably small, in the order of a few J mol^{-1}.

EXPERIMENTAL SECTION

Materials. (*S*,*S*,*S*)-D-BTA was prepared according to previously described procedures.[8,11] Heptane (spectrophotometric grade) was purchased from Acros and methylcyclohexane (MCH, spectrophotometric grade) was obtained from Aldrich. Isooctane (spectrophotometric grade) and decahydronaphthalene (synthesis grade, mixture of *cis* and *trans* isomers) were purchased from Merck.

Methods. Ultraviolet (UV) and CD measurements were simultaneously performed on a Jasco J-815 spectropolarimeter where the sensitivity, time constant, and scan rate were chosen appropriately. Corresponding temperature-dependent measurements were performed with a PFD-425S/15 Peltier-type temperature controller with a temperature range of 263−383 K and adjustable temperature slope. In all cases, a temperature slope of 1 K min^{-1} was used. For the measurements below 263 K, an Oxford Industries path cryostat was applied. The molar CD $\Delta\varepsilon$ was calculated from the CD effect as follows; $\Delta\varepsilon$ = CD effect/(32980·c·l) where the CD effect is given in mdeg, c is the concentration in mol L^{-1}, and l is the optical path length in cm (l = 1 mm, 0.5 or 1 cm). In all experiments, the linear dichroism was measured, and in all cases no linear dichroism was observed. Solutions were prepared by weighing the appropriate amount of (*S*,*S*,*S*)-D-BTA compound, after which this amount was transferred to a volumetric flask (flasks of 5 mL were employed). Then the flask was filled with the spectrophotometric grade solvent and put in an oscillation bath at 40 °C for 50 min, after which the flask was allowed to cool down. Any loss of solvent was compensated for. The solution infrared spectra were recorded with a Perkin-Elmer spectrum 1 and measured at a resolution of 4 cm^{-1}, by coadding 128 scans. Samples were held in a fixed path length (50 μm) cell with CaF_2 windows.

Model. In the model one monomer type, *S*, can aggregate into four different supramolecular polymer types, i.e., M^{35}, P^{35}, M^{45}, and P^{45}, where for each of the polymer types we assume a cooperative growth mechanism with nucleus size two. Such a cooperative growth is described by an equilibrium constant K_{nuc} for dimerization and equal equilibrium constants K_{elo} for all elongation steps within one type of polymer. The degree of cooperativity is given by the cooperativity factor σ defined as K_{nuc}/K_{elo}. Because both equilibrium constants may differ per aggregate type, these are labeled as K_{nuc}^{M35}, K_{nuc}^{M45}, K_{nuc}^{P35}, K_{nuc}^{P45}, K_{elo}^{M35}, K_{elo}^{M45}, K_{elo}^{P35}, and K_{elo}^{P45} for the M^{35}, P^{35}, M^{45}, and P^{45} polymers, respectively. We use the following thermodynamic parameters to describe the supramolecular polymerization process as a function of temperature: the enthalpy (ΔH_{elo}^{35}) and entropy (ΔS_{elo}^{35}) gain in elongation step of a 35° aggregate, the nucleation penalty (ΔH_{nuc}^{35}) for the formation of a 35° dimer, and the mismatch penalty (ΔH_{mmp}^{35}) for a monomer in a 35° aggregate with the nonpreferred (*P*-type) helicity, plus the same parameters for the 45° polymers. The mass-balance model is based on the principle of detailed balance, which states that in thermodynamic equilibrium also each individual reaction is in equilibrium. For instance, for the formation of the M^{35}-type nucleus $S + S \rightleftarrows M_2^{35}$, which has an equilibrium constant $K_{nuc}^{M35} = \sigma_{M35} K_{elo}^{M35}$, this implies that $[M_2^{35}] = \sigma_{M35} K_{elo}^{M35} s^2$, where s is the free monomer concentration in equilibrium. Similarly for the elongation reaction $M_2^{35} + S \rightleftarrows M_3^{35}$, with equilibrium constant K_{elo}^{M35}, it holds that $[M_3^{35}] = \sigma_{M35} (K_{elo}^{M35})^2 s^3$. In this way, the concentration of all types of polymers of all lengths can be expressed in terms of the free monomer concentration s. Since the sum of the free monomer concentration and that of all the monomers present in the different polymers should equal the total concentration s_{tot}, this yields (see Supporting Information (SI) for details) one equation with the free monomer concentration s as a single unknown:

$$s + \frac{\sigma_{M35} K_{elo}^{M35} s^2 (2 - K_{elo}^{M35} s)}{(1 - K_{elo}^{M35} s)^2} + \frac{\sigma_{P35} K_{elo}^{P35} s^2 (2 - K_{elo}^{P35} s)}{(1 - K_{elo}^{P35} s)^2} + \frac{\sigma_{M45} K_{elo}^{M45} s^2 (2 - K_{elo}^{M45} s)}{(1 - K_{elo}^{M45} s)^2} + \frac{\sigma_{P45} K_{elo}^{P45} s^2 (2 - K_{elo}^{P45} s)}{(1 - K_{elo}^{P45} s)^2} = s_{tot}$$

We solve these equations numerically using Matlab.

By expressing the equilibrium constants as $K_{elo}^{M35} = \exp(-(\Delta H_{elo}^{35} - T\Delta S_{elo}^{35})/RT)$, $K_{elo}^{M45} = \exp(-(\Delta H_{elo}^{45} - T\Delta S_{elo}^{45})/RT)$, $K_{elo}^{P35} = K_{elo}^{M35} \exp((\Delta H_{mmp}^{35} - T\Delta S_{mmp}^{35})/RT)$, and $K_{elo}^{P45} = K_{elo}^{M45} \exp(-(\Delta H_{mmp}^{45} - T\Delta S_{mmp}^{45})/RT)$, and the cooperativity factors as $\sigma_{M35} = \sigma_{P35} = \exp((\Delta H_{nuc}^{35} - T\Delta S_{nuc}^{35})/RT)$ and $\sigma_{M45} = \sigma_{P45} = \exp((\Delta H_{nuc}^{45} - T\Delta S_{nuc}^{45})/RT)$, the procedure can be repeated for various temperatures and for various concentrations S_{tot}, leading to Figures 7 and 9.

Fitting. The thermodynamic parameters ΔH_{elo}^{35}, ΔS_{elo}^{35}, ΔH_{mmp}^{35}, ΔS_{mmp}^{35}, ΔH_{nuc}^{35}, ΔS_{nuc}^{35}, and their counter parts for the 45° conformer were obtained by fitting the model results to the experimental melting curves obtained by temperature-dependent CD and temperature-dependent UV spectroscopy. The fitting consisted of a least-squares minimization of the differences between six experimental melting curves (both CD and UV at three different concentrations) and those calculated from the polymer concentrations as predicted by the model for a set of thermodynamic parameters. The theoretical UV melting curves were calculated as the total number of molecules present in supramolecular polymers multiplied by a UV signal per monomer, while the theoretical CD melting curves were calculated as the difference in the number of molecules present in right- and left-handed helices multiplied by a CD signal per monomer. These contributions per monomer were thus taken independent of the length of the polymers and independent of the overall concentration S_{tot}. Using Latin hypercube sampling, least-squares fittings were performed using Matlab from 100 random initial parameter sets. Parameters of the best fits for heptane, where the entropy terms ΔS_{mmp}^{35}, ΔS_{nuc}^{35}, ΔS_{mmp}^{45}, and ΔS_{nuc}^{45} were not fitted but taken as zero, are given in the captions of Figure 7. Those for MCH, where the 45° conformer is assumed absent, are given in the caption of Figure 9.

RESULTS

Solvent Effect on Thermodynamics of D-BTA Self-Assembly: Conformational Changes versus Helix Sense Inversion. We investigated the self-assembly of (*S*,*S*,*S*)-D-BTA in both linear (heptane) and branched (MCH) alkane solvents. CD and UV spectroscopic measurements were conducted between 363 K and a temperature close to the melting point of the solvent applied. The concentration of (*S*,*S*,*S*)-D-BTA was 3.0×10^{-5} M, and the solutions were cooled at a cooling rate of 1 K min^{-1}, ensuring that the self-assembly process occurs under thermodynamic equilibrium. An overlay of the CD cooling curves measured in MCH and heptane is shown in Figure 2. The dominance of negative CD-effects in heptane indicates a preference for *M* helical aggregates, while in MCH a switch in

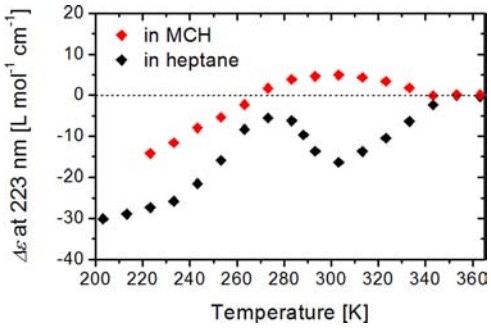

Figure 2. CD cooling curves of (*S*,*S*,*S*)-D-BTA in heptane (black) and in MCH (red) recorded at 223 nm with a cooling rate of 1 K min^{-1} and a concentration of 3.0×10^{-5} M.

helical preference is observed from *P* to *M* upon lowering the temperature. In heptane, the CD-effect reaches a plateau value around 210 K ($\Delta\varepsilon = -30$ L mol^{-1} cm^{-1}), while in MCH this plateau was not reached because of crystallization of the solvent.

The cooling curves in heptane and in MCH were investigated in more detail by analyzing the full CD and UV spectra measured at different temperatures. The results are shown in Figures 3 and 4. We first discuss the results obtained for heptane. To facilitate interpretation of the results, the CD and UV cooling curves were divided into four regimes I, II, III, and IV (Figure 3A,B). Regime I is above the aggregation temperature of 353 K, and all (*S*,*S*,*S*)-D-BTAs are present in a molecularly dissolved state. This is reflected by the absence of a CD signal and a UV absorption maximum at $\lambda = 208$ nm. Once the aggregation temperature is reached, (*S*,*S*,*S*)-D-BTA molecules start to aggregate as evidenced by a change in the λ_{max} in the UV spectra. In this regime II, the cooling curves of (*S*,*S*,*S*)-D-BTA obtained with CD spectroscopy differ significantly from those obtained with UV spectroscopy. This is in sharp contrast to the behavior in methyl-substituted BTAs where the cooling curves obtained with UV and CD spectroscopy are superimposable.[12] The almost linear decrease of the CD effect between 353 and 303 K is indicative for the presence of a dynamic equilibrium between different conformational states.[8] Analysis of the full CD spectra in regime II reveals a single, negative Cotton effect, indicative of a preference for conformer M_{45} (Figure 3C).[10] We previously attributed the dominance of this conformer to the participation of heptane molecules in the self-assembly process.[9,10] Regime III starts at 303 K, and no further changes are seen in the UV spectra indicating that (*S*,*S*,*S*)-D-BTA molecules are now fully aggregated. The $|\Delta\varepsilon|$, however, decreases starting from 303 K. In regime IV starting at 273 K, the shape of the CD spectra changes from a negative single to negative double Cotton effect. This indicates that now (*S*,*S*,*S*)-D-BTA is predominantly present in the conformer M_{35}.

In MCH, we can also distinguish four temperature regimes. The behavior in UV is highly similar to that observed in heptane, with the exception that aggregation starts at a slightly lower temperature (343 K). However, an even more pronounced discrepancy between the UV and CD cooling curves is visible (Figure 4A,B) since the CD effect first is positive and changes to negative upon cooling. In addition, below 343 K—the temperature at which aggregation starts—a double Cotton effect was observed at all temperatures. The latter indicates that a helical sense inversion occurred from *P* (P_{35}) to *M* (M_{35}), but the conformation within the columnar

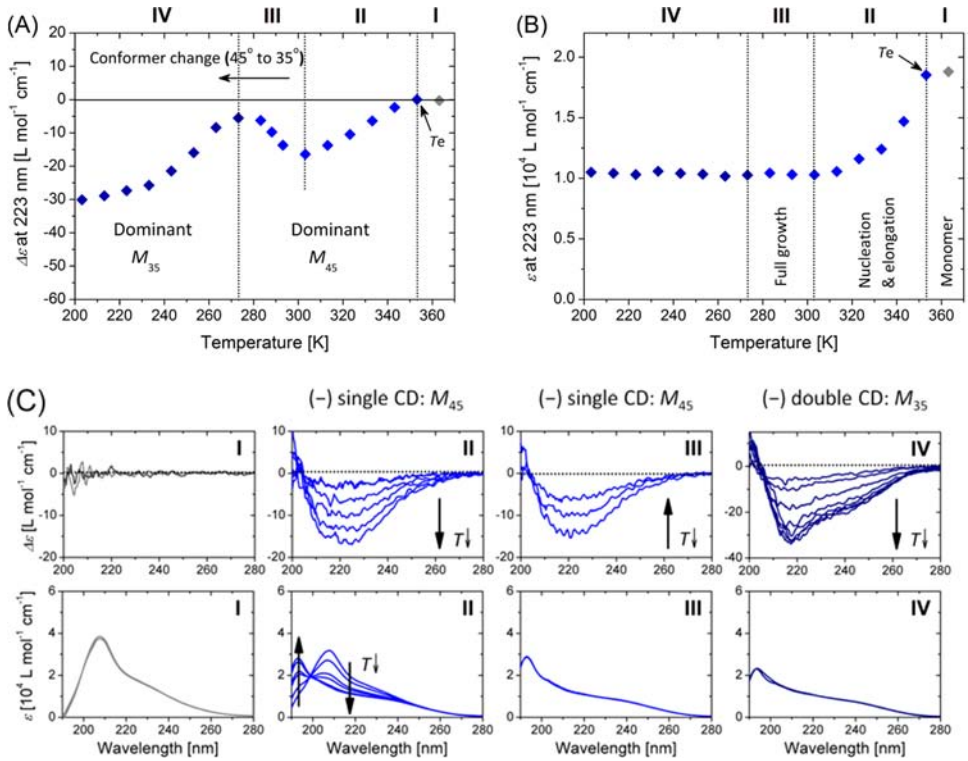

Figure 3. Cooling curves of (*S*,*S*,*S*)-D-BTA in heptane recorded with (A) CD and (B) UV spectroscopy probed at 223 nm with a cooling rate of 1 K min^{-1}. (C) Full CD and UV spectra in the individual temperature regimes I (363−353 K), II (343−303 K), III (293−273 K), and IV (263−203 K) at intervals of 10 K. Arrows indicate decreasing temperature. In all cases the concentration is 3.0×10^{-5} M.

dx.doi.org/10.1021/ja4073645 | J. Am. Chem. Soc. 2013, 135, 16497−16506

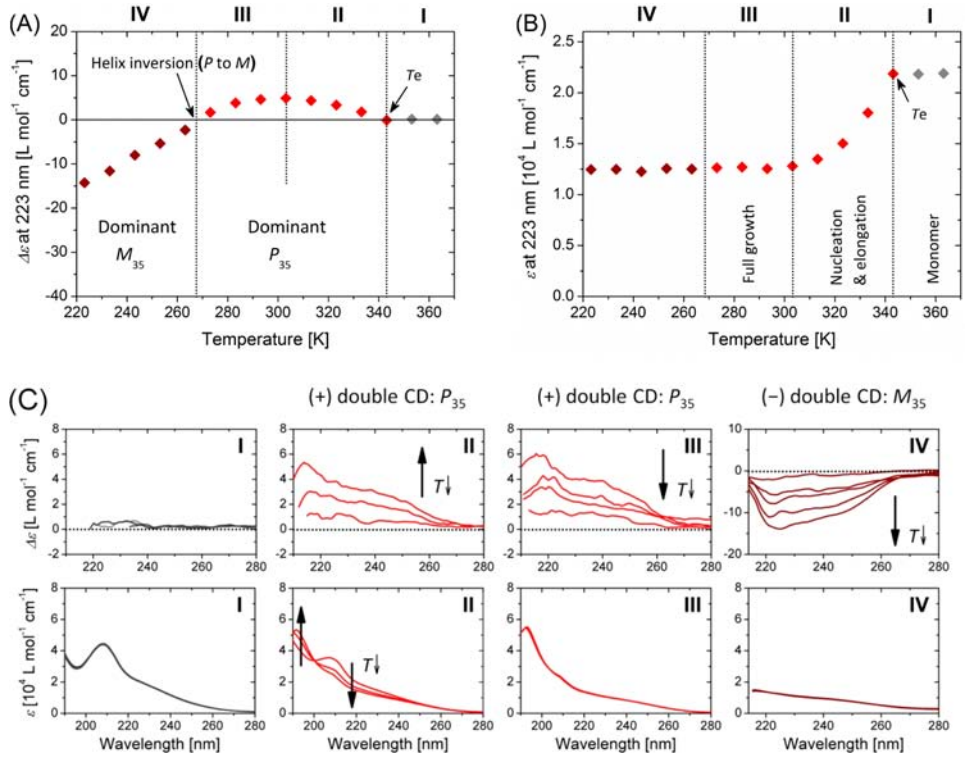

Figure 4. Cooling curves of (*S*,*S*,*S*)-D-BTA in MCH recorded with (A) CD and (B) UV spectroscopy probed at 223 nm with a cooling rate of 1 K min^{-1}. (C) Full CD and UV spectra in the individual temperature regimes I (363−343 K), II (333−313 K), III (303−273 K), and IV (263−223 K) at intervals of 10 K. Arrows indicate decreasing temperature. In all cases the concentration is 3.0×10^{-5} M.

aggregates kept the dihedral angle of 35°. In regime IV, the molecules are fully aggregated and $|\Delta\varepsilon|$ show a linear increase upon further cooling. Unfortunately, crystallization of the solvent prevented further cooling of the sample.

Thus, while heptane and MCH are both alkane solvents of similar polarity, they differently affect the self-assembly of (*S*,*S*,*S*)-D-BTAs. In heptane, the helical preference is always *M*, but a pronounced conformational change of the aggregate occurs which we attribute to the effective intercalation of the solvent within the aggregate. In contrast, in MCH the conformational preference is always the same, but a helical sense inversion takes place at 268 K. Interestingly, the concentration of the (*S*,*S*,*S*)-D-BTAs solutions in heptane or MCH has a very small effect on the temperatures at which either the conformational change (in heptane) or the helix inversion (for MCH) takes place (Figures 5 and S1). Similar tendencies were found in other solvents, i.e., a helical inversion between M_{35} and P_{35} could be observed in isooctane (branched alkane) and in decahydronaphthalene (bicyclic alkane) (Figures S2 and S3), and a conformer change from M_{45} to M_{35} could be observed in dodecane and other linear solvents (C6−C12).[9] The CD signal intensity (i.e., a preference of *P* over *M*) differs as does the temperature at which the transitions take place.

To substantiate the conclusions of CD spectroscopy, IR measurements both in MCH and heptane were performed for (*S*,*S*,*S*)-D-BTA at room temperature (293 K). The C═O stretching vibration can be evaluated with high sensitivity using IR spectroscopy. We previously established that different C═O stretch vibrations occur for BTAs that adopt a M_{45} and M_{35} conformation.[10] While M_{45} is characterized by a single peak at 1643 cm^{-1} with two small shoulders at 1630 and 1651 cm^{-1}, M_{35} shows two equally sized peaks at 1630 and 1645 cm^{-1} with one small shoulder at 1651 cm^{-1}. Figure 6 shows the amide I,

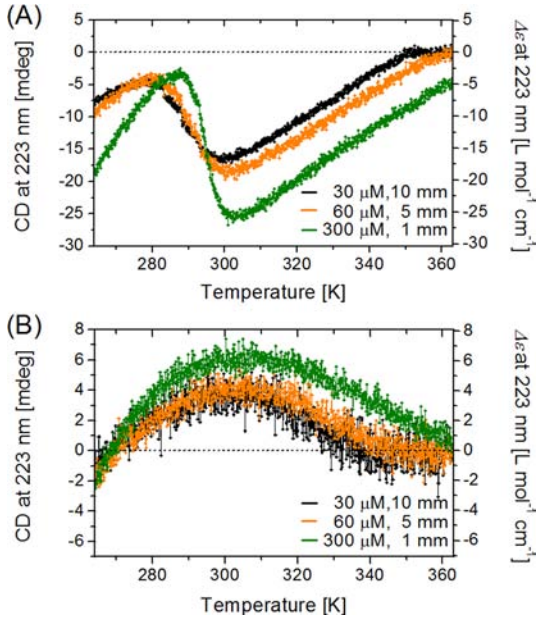

Figure 5. CD cooling curves of (*S*,*S*,*S*)-D-BTA probed at 223 nm (A) in heptane and (B) in MCH. In all cases, the cooling curves were recorded between 363 and 263 K and measured at 3.0×10^{-5} M, path length = 10 mm (black line), 6.0×10^{-5} M, path length = 5 mm (orange line), and 3.0×10^{-4} M, path length = 1 mm (green line).

amide II, and N−H stretch regions of the IR spectra recorded for (*S*,*S*,*S*)-D-BTA in MCH and heptane. Analysis of the IR spectra reveals a clear difference in the C═O stretching patterns between the two solvents, while the amide II peak at

dx.doi.org/10.1021/ja4073645 | J. Am. Chem. Soc. 2013, 135, 16497−16506

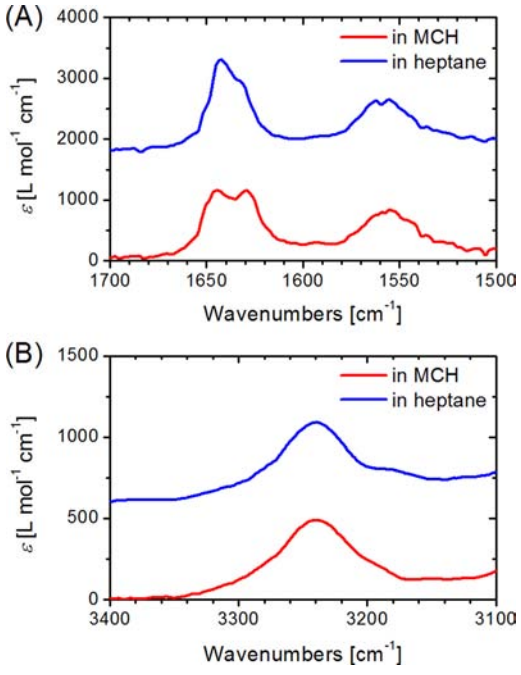

Figure 6. IR spectra recorded in (A) amide I (C═O stretching) and amide II (coupling of N−H bending and C−N stretching) region and (B) N−H stretching region of (*S*,*S*,*S*)-D-BTA in heptane (blue line) and in MCH (red line) at 1.8×10^{-3} M at 293 K. The heptane curves are shown with a 1800 L mol^{-1} cm^{-1} offset for (A) and a 600 L mol^{-1} cm^{-1} offset for (B).

1560 cm^{-1} and the N−H stretch at 3240 cm^{-1} are rather similar.

A Model to Describe Conformational and Helical Preferences in a Supramolecular Polymer. We recently put forward a model to describe a cooperative equilibrium polymerization of a monomer into a supramolecular polymer.[13] In this model—based on equilibriums between monomers, oligomers, and polymers— the aggregation process is divided into a nucleation regime and an elongation regime. The formation of a dimer is described by the equilibrium constant K_{nuc} for dimerization. In the elongation regime, where additional monomers add to the growing polymer chain, all equilibrium constants K_{elo} are assumed to be equal. The nucleation step is highly unfavorable, so that $K_{nuc} \ll K_{elo}$. The degree of cooperativity in the supramolecular polymerization is given by the cooperativity factor σ defined as K_{nuc}/K_{elo}. Increasingly small numbers for σ indicate an increasingly cooperative system. This model allowed quantification of the thermodynamic parameters of supramolecular polymerizations, including the measure of cooperativity in a number of different systems.[14]

Here we extend this model to describe the cooperative supramolecular polymerization of one monomer type that can form two types of polymers (35° and 45°) both with two types of helicities (*P* and *M*). Thus, this model enables a description of the polymerization of (*S*,*S*,*S*)-D-BTAs in either heptane or MCH as a function of temperature. We assume that the activation step in the supramolecular polymerization is the formation of a dimer. We use the following thermodynamic parameters to describe the supramolecular polymerization process as a function of temperature: the enthalpy (ΔH^{35}_{elo}) and entropy (ΔS^{35}_{elo}) gain in elongation step of a 35° aggregate, the nucleation penalty (ΔH^{35}_{nuc}) for the formation of a 35° dimer, and the mismatch penalty (ΔH^{35}_{mmp}) for a monomer in a 35° aggregate with the nonpreferred (*P*-type) helicity, plus the same parameters for the 45° polymers.

The best fit of this model to the temperature-dependent experimental CD and UV data of (*S*,*S*,*S*)-D-BTA in heptane is shown in Figure 7A. The UV and CD cooling curves for all three concentrations were fit with the model together, resulting in a single set of thermodynamic parameters as given in the caption of Figure 7. For the lowest two concentrations, the model fits both the CD and the UV data very well. In addition, for the highest concentration, the features of the experimental cooling curve are also well captured, although there is some deviation. Calculation of the equilibrium constants *K* from the thermodynamic parameters reveals the tiny variations in stability between the different conformers. In heptane at 270 K for example, when all conformers coexist in solution, the K_{elo} is 6.1839×10^7 M^{-1} for M_{35}, while K_{elo} is 6.1079×10^7 M^{-1} for P_{45} (Table 1). The difference between the equilibrium constants of the most (M_{35}) and least (P_{45}) abundant helical

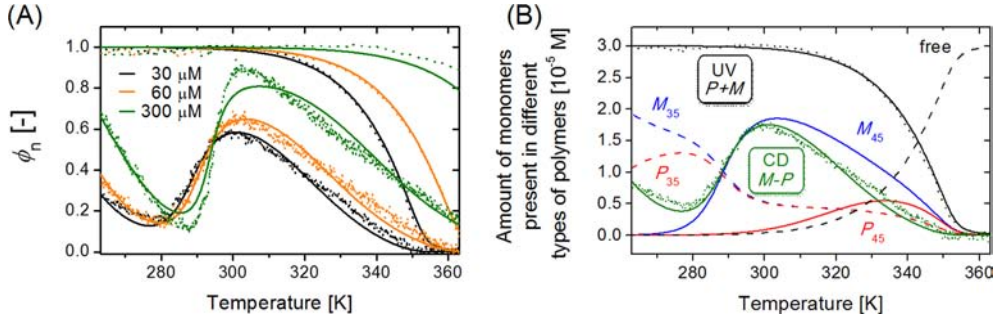

Figure 7. Fits of the CD and UV cooling curves for solutions of (*S*,*S*,*S*)-D-BTA in heptane, based on CD and UV data from Figures 5A and S1A. (A) Net helicity or degree of aggregation (ϕ_n) (dotted lines) as a function of temperature at the three different concentrations, i.e., 3.0×10^{-5} M (black), 6.0×10^{-5} M (orange), and 3.0×10^{-4} M (green) and fits for the CD and UV cooling curves (solid lines). The thermodynamic parameters obtained by the fit are: $\Delta^{35}_{elo} = -72.691$ kJ mol^{-1}, $\Delta S^{35}_{elo} = -0.12006$ kJ mol^{-1} K^{-1}, $\Delta H^{35}_{mmp} = -0.000076$ kJ mol^{-1}, $\Delta H^{35}_{nuc} = -22.822$ kJ mol^{-1}, $\Delta H^{45}_{elo} = -72.628$ kJ mol^{-1}, $\Delta S^{45}_{elo} = -0.11985$ kJ mol^{-1} K^{-1}, $\Delta H^{45}_{mmp} = -0.02238$ kJ mol^{-1}, and $\Delta H^{45}_{nuc} = -20.467$ kJ mol^{-1}. (B) For the 3.0×10^{-5} M solution the amount of monomers present in each of the different polymer species M_{45} (solid blue), M_{35} (dashed blue), P_{45} (solid red), and P_{35} (dashed red) is shown as well as the sum of these amounts (solid black line corresponding to UV signal, with the experimental UV data represented by a dotted black line) and difference between the amounts in left and right handed helices (solid green line corresponding to CD signal, with the experimental CD data represented by a dotted green line); the dashed black line corresponds to the free monomer concentration.

dx.doi.org/10.1021/ja4073645 | J. Am. Chem. Soc. 2013, 135, 16497−16506

Table 1. Equilibrium Constants K_{elo} Calculated for (*S*,*S*,*S*)-D-BTA Present in Different Helical Conformations and the Amount of Monomers in Different Types of Polymer at 3.0 × 10^{-5} M in Heptane and MCH

heptane				
T [K]	K_{elo} [M^{-1}]			
	M_{35}	P_{35}[a]	M_{45}[a]	P_{45}[a]
270	6.1839 × 10^7	× 0.999966	× 0.997599	× 0.987703
330	1.7156 × 10^5	× 0.999972	× 1.002671	× 0.994526
Amount of Monomers in Different Types of Polymer [× 10^{-5} M]				
270	1.7270	1.2440	0.0265	0.0011
330	0.3682	0.3671	1.1600	0.5335
MCH				
T [K]	K_{elo} [M^{-1}]			
	M_{35}	P_{35}[a]		
270	1.4963 × 10^7	× 1.000049		
330	6.2935 × 10^4	× 1.002346		
Amount of Monomers in Different Types of Polymer [× 10^{-5} M]				
270	1.4880	1.5050		
330	0.7371	0.7854		

[a]The small differences in K_{elo} are highlighted by giving the value for the M_{35} conformer and relate to the values for the other conformers by a multiplication factor.

conformation is very small and corresponds to a free energy difference of 28 J mol^{-1} only.

Importantly, the model allows gathering information on the amounts of different polymer species formed at the different temperatures and concentrations (Table 1). Figure 7B, for instance, shows the amount of monomers present in the different polymer species as a function of temperature for a concentration of 3.0 × 10^{-5} M (Figure S4 for the higher concentrations). These speciation plots show that (i) at the elongation temperature, all four polymer types (M_{35}, P_{35}, M_{45}, P_{45}) appear immediately; (ii) initially both *P* and *M* occur in equal amounts such that the CD signal remains zero for a while; and (iii) at lower temperatures, the *M*-helicity of 45° type aggregates becomes most abundant, explaining the initial increase in CD signal. Around T = 290 K, the 35° conformer takes over, and both helicities occur in almost equal amounts, which initially results in a lower CD signal. When the temperature decreases further, the *M*-helicity becomes more favorable and increases the CD signal again. The takeover of 35° conformer below T = 290 K is explained by the fact that although the changes in free energy on elongation for the two stack types are almost equal at all temperatures (Figure 8A), at 290 K, ΔG^{35}_{nuc} becomes more negative than ΔG^{45}_{elo}. This is reflected by the difference $\Delta G^{45}_{elo} - \Delta G^{35}_{elo}$ which becomes larger than 0 below T = 290 K (Figure 8B).

In a similar fashion, the temperature-dependent UV (Figure S1B) and CD (Figure 5B) curves measured in MCH were fitted for the three different concentrations (3.0 × 10^{-5}, 6.0 × 10^{-5}, and 3.0 × 10^{-4} M) together. In contrast to the heptane case, entropic contributions of the nucleation and mismatch penalty are used as well. Hence, the nucleation and mismatch penalty are taken temperature dependent using $\Delta G = \Delta H - T\Delta S$. In MCH only the 35° conformer occurs; as a result, only these conformers were considered in the model, and the superscript 35 for the parameters is omitted here. The model thus uses the following parameters: enthalpy gain in elongation step (ΔH_{elo}), entropy gain in elongation step ((ΔS_{elo})), enthalpy ((ΔH_{nuc})) and entropy (ΔS_{nuc}) of the nucleation penalty for a dimer, and the enthalpy (ΔH_{mmp}) and entropy (ΔS_{mmp}) of the mismatch penalty for a monomer in an aggregate with the nonpreferred (*P*-type) helicity. The fit to the experimental UV and CD data is shown in Figure 9A, and the thermodynamic parameters derived are shown in the caption of Figure 9. For example, calculation of the equilibrium constants at 330 K reveals that K_{elo} is 6.3082 × 10^4 M^{-1} for P_{35}, while K_{elo} is 6.2935 × 10^4 M^{-1} for M_{35}, indicating a difference in stability of only 6 J mol^{-1} between the two conformational states (Table 1). Plots specifying the abundances of the different polymer species for concentrations of 3.0 × 10^{-5}, 6.0 × 10^{-5}, and 3.0 × 10^{-4} M are given in Figures 9B, S5A, and S5B, respectively.

Upon cooling, an almost linear increase in CD with decreasing temperature is observed, and the relative abundance of *P* and *M* helical polymers is very similar. This causes a notable difference in temperature when CD and UV start to deviate from zero: the CD signal appears well below T_e because the abundance of *P* and *M* is initially the same. Between 330 and 268 K, a slight excess of *P* over *M* is observed, but this changes below 268 K. The origin of the CD signal switching sign around T = 268 K (which is independent of concentration) can be traced back to a switch in the sign of the mismatch penalty $\Delta G_{mmp} = \Delta H_{mmp} - T\Delta S_{mmp}$ (Figure S6).

Analysis of the Free Energies ΔG Involved in BTA Self-Assembly. In order to rationalize the observed differences in helical bias and conformational preference when BTA-based monomers self-assemble in a helical columnar stack, we first analyze the temperature-dependent behavior of BTA self-assembly in terms of free energy. Figure 10A shows the free

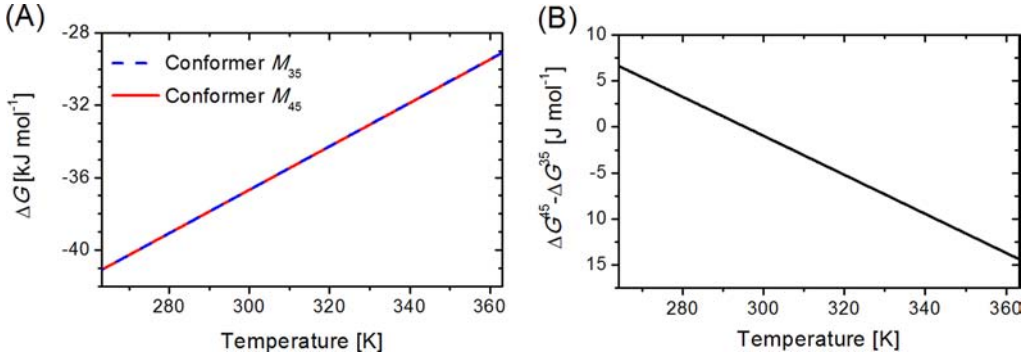

Figure 8. (A) Temperature-dependent Gibbs free energy of two conformers M_{35} and M_{45}. (B) The difference in Gibbs free energy between M_{35} and M_{45} as a function of temperature. Note that the *y*-axis is in J mol^{-1}.

dx.doi.org/10.1021/ja4073645 | J. Am. Chem. Soc. 2013, 135, 16497−16506

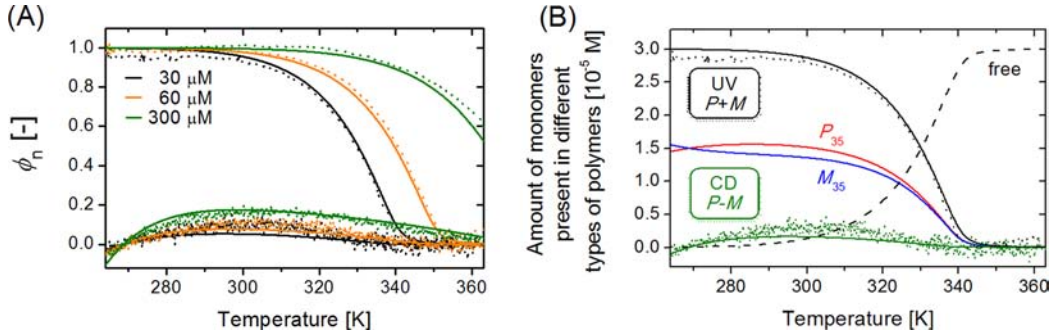

Figure 9. Fits of the CD and UV cooling curves for solutions of (*S*,*S*,*S*)-D-BTA in MCH, based on CD and UV data from Figures 5B and S1B. (A) Net helicity or degree of aggregation (ϕ_n) (dotted lines) as a function of temperature at the three different concentrations, i.e. 3.0×10^{-5} M (black), 6.0×10^{-5} M (orange) and 3.0×10^{-4} M (green) and fits for the CD and UV cooling curves (solid lines). The thermodynamic parameters obtained by the fit are; $\Delta H_{elo} = -67.553$ kJ mol^{-1}, $\Delta S_{elo} = -0.11283$ kJ mol^{-1} K^{-1}, $\Delta H_{mmp} = -0.02832$ kJ mol^{-1}, $\Delta S_{mmp} = -0.0001053$ kJ mol^{-1} K^{-1}, $\Delta H_{nuc} = 23.579$ kJ mol^{-1}, and ΔS_{nuc} 0.12139 kJ mol^{-1}. (B) For the 3.0×10^{-5} M solution the amount of monomers present in each of the different polymer species P_{35} (solid red) and M_{35} (solid blue) is shown as well as the sum of these amounts (solid black line corresponding to UV signal, with the experimental UV data represented by a dotted line) and difference between the amounts in left and right handed helices (solid green line corresponding to CD signal, with the experimental CD data represented by a dotted green line); the dashed black line corresponds to the free monomer concentration.

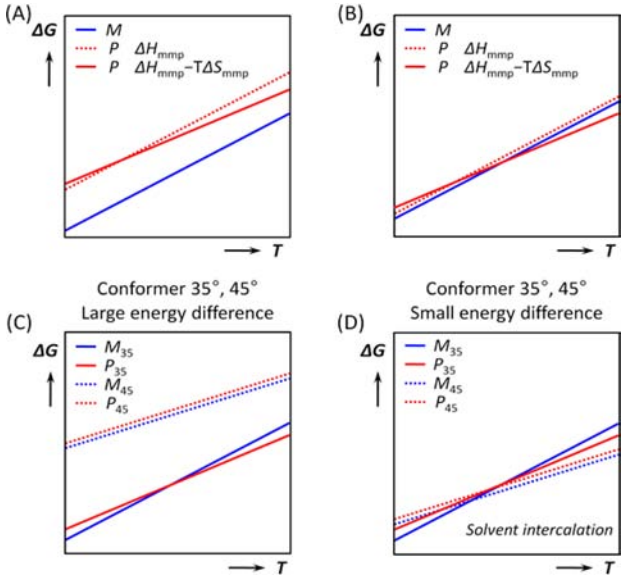

Figure 10. Schematic of the behavior of temperature-dependent free energies of different conformers and different helicities. (A) Situation with one conformer that can adopt two helicities with a preference for *M*-type helicity (blue line) and a constant mismatch penalty (red dotted line) or a temperature-dependent mismatch penalty (red line). (B) Situation as (A) but for a small mismatch penalty a temperature-dependent mismatch penalty may result in an intersection of the free energies, giving rise to a critical temperature where the preferred helicity changes. (C) Same situation as (B) with the temperature-dependent mismatch penalty, but with a second conformer present that does not play a role, as its energy (for both helicities) is much higher. (D) In case the energy difference between the two conformers is small, there might be another critical temperature where one conformer takes over from the other.

energy ΔG as a function of the temperature when chiral methyl-substituted BTA monomers self-assemble into stacks of a single helical type. Depending on the configuration of the chiral center, methyl-substituted BTAs form *P* or *M* helical stacks. Assume that the chiral monomer has a preference for the *M*-type helicity, illustrated by the lower values for ΔG in Figure 10A. Then, the gain in free energy on addition of a monomer to a stack is always larger for the *M*-type stacks than for the *P*-type stacks. In our model, this is represented by an enthalpy mismatch penalty ΔH_{mmp} which is temperature independent.[13a] A temperature dependence can be incorporated by adding a ΔS term to the mismatch penalty, i.e., $\Delta G_{mmp} = \Delta H_{mmp} - T\Delta S_{mmp}$. Whereas for a constant mismatch penalty the line for ΔG (red dotted line) remains parallel to that of the preferred helicity, for a temperature-dependent mismatch penalty (solid red line) the lines will eventually intersect. However, as long as the $T\Delta S_{mmp}$ term is relatively small as compared to ΔH_{mmp}, the temperature effect can be ignored, and the *M*-type helicity remains preferred at all realistic temperatures. However, when the mismatch penalty ΔH_{mmp} becomes small, the preferences for a monomer to self-assemble in either *P* or *M* helical columnar aggregates come closer together as illustrated in Figure 10B. For a stereogenic center in which the difference between the two substituents becomes very small, as is the case for D−H isotope-induced chirality, this preference for either *P* or *M* helical stacks becomes indeed less pronounced as shown in several systems.[8,1a] If there is a temperature dependence for this case with a small ΔH_{mmp}, the two lines describing the ΔG of the *P*- and *M*-type stacks as a function of temperature may intersect within the temperature range considered, resulting in a critical temperature above which the *P*-type stacks are more favorable, whereas below this temperature *M*-type stacks are preferred; exactly the behavior we observe in MCH for (*S*,*S*,*S*)-D-BTA.

Apart from the possibility of forming *P*- or *M*-type helical stacks, there can also be two different conformers with a 35° or 45° angle that can adopt either *P*- or *M*-type helicity. If one of these two conformers (45°) is energetically less favorable than the other (35°), as is the case in Figure 10C, the former will hardly be present. This system then still behaves exactly the same as the one with the temperature-dependent mismatch penalty depicted in Figure 10B, meaning that one conformer dominates, but a shift in the helical preference can occur upon changing the temperature. However, if the energy difference between the two conformers is smaller, e.g., as a result of an additional interaction stabilizing the less favorable conformer, the ΔGs of the two conformers may intersect as well (Figure 10D). As a result, at the highest temperature the M_{45} conformer is most favorable (such that CD effect increases with decreasing temperature as more and more monomers are forming M_{45}

dx.doi.org/10.1021/ja4073645 | J. Am. Chem. Soc. 2013, 135, 16497−16506

stacks), but if the temperature decreases, all ΔGs come closer such that the various stack types will all be formed (such that the CD-effect decreases). If the temperature decreases further, the M_{35} becomes most favorable (such that the CD-effect increases again). This behavior is exactly what we observe in heptane. At temperatures above 303 K, heptane molecules are intercalated in the helical stacks and favor the formation of the M_{45} conformation. Upon decreasing the temperature, however, the heptane molecules are expelled from the stacks, and the bias for *M* helicity decreases. Below 273 K, M_{35} becomes the more dominant conformer.

DISCUSSION

The importance of the molecular structure of solvent molecules in aggregation processes and helical polymer conformations is receiving more and more attention. For example, optically active solvents were found to induce a preferred helical conformation in achiral conjugated polymers,[15] helical polyisocyanates,[16] bipyridine-based discotics,[17] and tubular structures.[18] In addition, small changes in the solvent polarity can reverse the helical sense preference in polyisocyanates[16] and polyquinoxalines.[19]Also in supramolecular polymerization processes, tiny differences in solvent structure affect the thermodynamics of the self-assembly process noticeably.[20]

Our above analysis nicely illustrates that the helical and conformational preferences in D-BTA self-assembly are governed by tiny energy differences, and the molecular structure of the solvent plays a dominant role. However, it does not elucidate their molecular origin. Recently, we performed plane-wave DFT calculations to get insight into the molecular origin of the isotope-induced diastereomeric enrichment in D-BTA-based supramolecular polymers.[21] The creation of a chiral center with *S*-configuration on the α-position of the ethyl chains of a BTA by H/D exchange resulted in a small but notable preference for the formation of a *P*-helical supramolecular polymer. The preference was directly related to the difference between the zero-point energies of the two diastereomerically related BTA aggregates at the supramolecular level. Analysis of the results revealed that the most favorable situation is reached when the C−D vibrations point toward regions of higher electron density (i.e., the strongly electronegative oxygen atom) and the C−H vibrations point toward regions of lower electron density in the D-BTA-based supramolecular polymers. This situation is present when (*S*,*S*,*S*)-D-BTA adopts a *P*-helical conformation. In MCH, a solvent that does not intercalate between the BTAs, indeed a small preference for *P*-helical conformation is found, in line with the DFT results. However, lowering the temperature below 268 K changes this preference.

The above-mentioned DFT calculations were performed in vacuum, therefore the effect of solvent was not taken into account. Upon adding a solvent, entropy changes of the solvent as well as the supramolecular aggregate may play a role. In fact, it is well-known that the free energy differences between different protein conformations are more determined by the overall change in entropy of the solvent than by the change in entropy of the protein.[22] We assume that the difference in the change in entropy of the solvent upon interchange of hydrogen with deuterium in D-BTAs is negligible. As such, the dominant contribution to the change in entropy will be from the supramolecular aggregate and specifically from its vibrational frequencies. The cause of the aforementioned temperature dependence of the helical preference may then be found in considering the zero-point energy as well as any thermal excitations of these vibrational frequencies.

Dunitz and Ibberson recently reported that the unit cell of solid C_6H_6 is smaller than that of C_6D_6 above 170 K.[23] Although the zero-point energy always leads to a smaller effective size for a deuterium than that for a hydrogen, it has been shown that in systems with low-frequency vibrations, the temperature effect expands the effective size of a deuterium faster than that of a hydrogen. A similar study has been conducted by Lacks, in which the ratio in molar volume between C−D and C−H in crystalline polyethylene was studied by means of ab initio calculations as well as experimentally.[24] Herein, anharmonic corrections were taken into account. Their calculations show that at room temperature (T = 300 K) the high-frequency C−H and C−D stretching vibrations approach the classical harmonic limit and are the dominant contributors to the molar volume; however, with decreasing temperature the contribution of low-frequency lattice modes starts to increase. Although these experiments show that by changing the temperature, the ratio of the molar volumes of protium versus deuterium can invert, tentatively suggesting that a similar phenomenon could lead to a change in the preference for the helical bias within the BTA supramolecular system, they do not provide an explanation to what extent the solvent plays a role in this mechanism.

O'Leary and co-workers studied in detail the origin of the equilibrium isotope effect observed in the racemization of Mislov's bridged biphenyl compounds.[25] Depending on the molecular structure of the biphenyls, Mislow's experimental work revealed both normal and inverse kinetic isotope effects.[26] In addition, an intriguing and unexplained solvent effect was reported wherein the racemization in heptane was faster than in benzene at higher temperatures, but the reverse was found at lower temperatures.[26b] The analysis by O'Leary et al. partitions the underlying contributions to the observed kinetic isotope effects into an enthalpic correction from the zero-point energy and vibrations as well as entropic corrections arising from vibrations, rotations, and translations. The results show that the overall kinetic isotope effect is caused by a complex interplay of these enthalpic and entropic factors and sensitively depends on the molecular structure of the compounds. In addition, the difference in vibrational enthalpic corrections is dominated by the differences in frequencies lower than 800 cm^{-1}. Based on the particular nature of the vibrational frequencies, the enthalpic corrections can lead to a normal or inverse kinetic isotope effect. The entropic corrections on the other hand may change this as a result of the temperature. Indeed, by either raising or lowering the temperature, the sign of the Gibbs free energy difference term can be switched and dominant entropic contributions can give rise to unusual kinetic isotope effects. The effect of solvent, however, was not taken into account in this analysis.

On the basis of this observation, a hypothesis can be formed regarding the helical preferences in (*S*,*S*,*S*)-D-BTAs and the influence of the solvent in this process. The overall helical preference is determined by the Gibbs free energy. The contribution of the low wavenumber frequencies (i.e., the lattice modes) is known from statistical thermodynamics to be dominant for the vibrational enthalpic and entropic terms. It has been shown that even solvents which do not form bonds with the solute (i.e., noninteracting solvents) are able to cause significant changes in the low-frequency lattice modes.[27] By changing the temperature of the system, the entropic correction

dx.doi.org/10.1021/ja4073645 | J. Am. Chem. Soc. 2013, 135, 16497−16506

changes accordingly, leading to a different equilibrium between the two diastereomers. Similarly, by changing the solvent, the sign and magnitude of both the enthalpic and entropic corrections change as a consequence of the change in the low-frequency lattice modes. Consequently, a completely different trend in the cooling curves can be found.

CONCLUSIONS

The results presented here show that isotope substitution allows to sensitively probe solvophobic effects in supramolecular aggregation. (*S*,*S*,*S*)-D-BTAs self-assemble in alkane solvents into helical, one-dimensional, supramolecular polymers, the conformation of which is dictated by solvent structure and temperature. In MCH, the aggregation process is dominated by the presence of 35° conformations of opposite sense: At high temperatures *P* helical polymers dominate, while lowering the temperature results in a preference of *M* helical polymers below 268 K. In heptane, the four conformational states are in equilibrium, and their relative abundances depend sensitively on the temperature. At all temperatures, the *M* helical state is dominant, but lowering the temperature results in a switch between a preference for the 45° to a 35° dihedral angle.

We developed a model based on the equilibrium between monomers and polymers in the different conformational states to understand the conformational changes that (*S*,*S*,*S*)-D-BTAs show as a response to temperature and solvent. A good agreement between the model fits and the experimental data allows us to quantify the thermodynamic parameters that characterize the different conformational states in heptane and MCH, and from those, the amount of the species that occur at different stages of the polymerization process. Analysis of the results shows that the change in helical preference of (*S*,*S*,*S*)-D-BTA supramolecular polymers in MCH can be attributed to a mismatch penalty that depends on the temperature. We propose that this temperature dependence is related to the entropy of the solvent−solute interactions, which results in a different bias of the helical sense as a consequence of influencing low-frequency vibrations. In heptane, intercalation of the solvent into the helical stacks stabilizes the 45° dihedral angle conformation above 303 K. Lowering the temperature changes the conformational preference to a 35° dihedral angle and reduces the preference for the *M* helical sense.

While the differences in stability are very small, in the order of a few J mol^{-1}, the impact they have on the relative abundances of the different types of conformers formed by (*S*,*S*,*S*)-D-BTAs is significant. This shows that small effects can be strongly amplified in cooperatively aggregating systems and that the combination of interactions between the solvent/supramolecular aggregate, temperature, and solvent structure is a factor that cannot be ignored in supramolecular polymerizations. A complete rationalization of the observed effects on a molecular level, however, is not yet straightforward as a subtle balance between the vibrational enthalpic and entropic term of the isotope effect is present.

ASSOCIATED CONTENT

Supporting Information

Additional UV, CD and IR spectra of (*S*,*S*,*S*)-D-BTA, fits of the T-dependent UV and CD data and the corresponding speciation plots, comparison between deuterated and achiral BTA self-assemblies and a description of the equilibrium model. This material is available free of charge via the Internet at http://pubs.acs.org.

AUTHOR INFORMATION

Corresponding Authors

*a.palmans@tue.nl
*e.w.meijer@tue.nl

Notes

The authors declare no competing financial interest.

ACKNOWLEDGMENTS

This research was funded by the Ministry of Education, Culture and Science (Gravity program 024.001.035), The Netherlands Organization for Scientific Research (NWO) and the European Research Council (FP7/2007−2013) ERC Grant Agreement. H.t.E. and A.M. thank Prof. P. Hilbers for the opportunity to do this research.

REFERENCES

(1) (a) Barth, G.; Djerassi, C. *Tetrahedron* **1981**, *37*, 4123−4142. (b) Green, M. M.; Peterson, N. C.; Sato, T.; Teramoto, A.; Cook, R.; Lifson, S. *Science* **1995**, *268*, 1860−1866. (c) Berger, R.; Laubender, G.; Quack, M.; Sieben, A.; Stohner, J.; Willeke, M. *Angew. Chem., Int. Ed.* **2005**, *44*, 3623−3626. (d) Barabas, B.; Caglioti, L.; Micskei, K.; Zucchi, C.; Palyi, G. *Origins Life Evol. Biospheres* **2008**, *38*, 317−327. (e) Kawasaki, T.; Matsumura, Y.; Tsutsumi, T.; Suzuki, K.; Ito, M.; Soai, K. *Science* **2009**, *324*, 492−495. (f) Soai, K.; Shibata, T.; Morioka, H.; Choji, K. *Nature* **1995**, *378*, 767−768. (g) Soai, K.; Shibata, T.; Sato, I. *Acc. Chem. Res.* **2000**, *33*, 382−390. (h) Haesler, J.; Schindelholz, I.; Riguet, E.; Bochet, C. G.; Hug, W. *Nature* **2007**, *446*, 526−529.

(2) (a) Anet, F. A. L.; Kopelevich, M. *J. Am. Chem. Soc.* **1986**, *108*, 1355−1356. (b) Saunders, M.; Wolfsberg, M.; Anet, F. A. L.; Kronja, O. *J. Am. Chem. Soc.* **2007**, *129*, 10276−10281. (c) Anet, F. A. L.; Kopelevich, M. *J. Am. Chem. Soc.* **1986**, *108*, 2109−2110. (d) Carr, C. A.; Ellison, S. L. R.; Robinson, M. J. T. *Tetrahedron Lett.* **1989**, *30*, 4585−4588. (e) Forsyth, D. A.; Hanley, J. *J. Am. Chem. Soc.* **1987**, *109*, 7930−7932. (f) Forsyth, D. A.; Prapansiri, V. *Tetrahedron Lett.* **1988**, *29*, 3551−3554.

(3) Green, M. M.; Andreola, C.; Munoz, B.; Reidy, M. P.; Zero, K. *J. Am. Chem. Soc.* **1988**, *110*, 4063−4065.

(4) (a) Mugridge, J. S.; Bergman, R. G.; Raymond, K. N. *Angew. Chem., Int. Ed.* **2010**, *49*, 3635−3637. (b) Mugridge, J. S.; Bergman, R. G.; Raymond, K. N. *J. Am. Chem. Soc.* **2010**, *132*, 1182−1183. (c) Mugridge, J. S.; Bergman, R. G.; Raymond, K. N. *J. Am. Chem. Soc.* **2012**, *134*, 2057−2066. (d) Felder, T.; Schalley, C. A. *Angew. Chem., Int. Ed.* **2003**, *42*, 2258−2260. (e) Haino, T.; Fukuta, K.; Iwamoto, H.; Iwata, S. *Chem.—Eur. J.* **2009**, *15*, 13286−13290. (f) Rechavi, D.; Scarso, A.; Rebek, J. *J. Am. Chem. Soc.* **2004**, *126*, 7738−7739. (g) Zhao, Y. L.; Houk, K. N.; Rechavi, D.; Scarso, A.; Rebek, J. *J. Am. Chem. Soc.* **2004**, *126*, 11428−11429.

(5) (a) Giagou, T.; Meyer, M. P. *Chem.—Eur. J.* **2010**, *16*, 10616−10628. (b) Gómez-Gallego, M.; Sierra, M. A. *Chem. Rev.* **2011**, *111*, 4857−4963. (c) Bennet, A. J. *Curr. Opin. Chem. Biol.* **2012**, *16*, 472−478.

(6) Wiberg, K. B. *Chem. Rev.* **1955**, *55*, 713−743.

(7) Wade, D. *Chem. Biol. Interact.* **1999**, *117*, 191−217.

(8) Cantekin, S.; Balkenende, D. W. R.; Smulders, M. M. J.; Palmans, A. R. A.; Meijer, E. W. *Nat. Chem.* **2011**, *3*, 42−46.

(9) Cantekin, S.; Nakano, Y.; Everts, J. C.; van der Schoot, P.; Meijer, E. W.; Palmans, A. R. A. *Chem. Commun.* **2012**, *48*, 3803−3805.

(10) Nakano, Y.; Hirose, T.; Stals, P. J. M.; Meijer, E. W.; Palmans, A. R. A. *Chem. Sci.* **2012**, *3*, 148−155.

(11) Balkenende, D. W. R.; Cantekin, S.; Duxbury, C. J.; van Genderen, M. H. P.; Meijer, E. W.; Palmans, A. R. A. *Synth. Commun.* **2012**, *42*, 563−573.

(12) (a) Smulders, M. M. J.; Schenning, A. P. H. J.; Meijer, E. W. *J. Am. Chem. Soc.* **2008**, *130*, 606−609. (b) Stals, P. J. M.; Smulders, M. M. J.; Martin-Rapún, R.; Palmans, A. R. A.; Meijer, E. W. *Chem.—Eur. J.* **2009**, *15*, 2071−2080.
(13) (a) Markvoort, A. J.; ten Eikelder, H. M. M.; Hilbers, P. A. J.; de Greef, T. F. A.; Meijer, E. W. *Nature Commun.* **2011**, *2*, 509−517. (b) Zhao, D. H.; Moore, J. S. *Org. Biomol. Chem.* **2003**, *1*, 3471−3491.
(14) (a) Cantekin, S.; ten Eikelder, H. M. M.; Markvoort, A. J.; Veld, M. A. J.; Korevaar, P. A.; Green, M. M.; Palmans, A. R. A.; Meijer, E. W. *Angew. Chem., Int. Ed.* **2012**, *51*, 6426−6431. (b) ten Eikelder, H. M. M.; Markvoort, A. J.; de Greef, T. F. A.; Hilbers, P. A. J. *J. Phys. Chem. B* **2012**, *116*, 5291−5301. (c) Wang, F.; Gillissen, M. A. J.; Stals, P. J. M.; Palmans, A. R. A.; Meijer, E. W. *Chem.—Eur. J.* **2012**, *18*, 11761−11770.
(15) (a) Nakano, Y.; Liu, Y.; Fujiki, M. *Polym. Chem.* **2010**, *1*, 460−469. (b) Kawagoe, Y.; Fujiki, M.; Nakano, Y. *New J. Chem.* **2010**, *34*, 637−647. (c) Nakashima, H.; Koe, J. R.; Torimitsu, K.; Fujiki, M. *J. Am. Chem. Soc.* **2001**, *123*, 4847−4848.
(16) Green, M. M.; Khatri, C.; Peterson, N. C. *J. Am. Chem. Soc.* **1993**, *115*, 4941−4942.
(17) Palmans, A. R. A.; Vekemans, J. A. J. M.; Havinga, E. E.; Meijer, E. W. *Angew. Chem., Int. Ed.* **1997**, *36*, 2648−2651.
(18) Isare, B.; Linares, M.; Zargarian, L.; Fermandjian, S.; Miura, M.; Motohashi, S.; Vanthuyne, N.; Lazzaroni, R.; Bouteiller, L. *Chem.—Eur. J.* **2010**, *16*, 173−177.
(19) Yamada, T.; Nagata, Y.; Suginome, M. *Chem. Commun.* **2010**, *46*, 4914−4916.
(20) (a) Jonkheijm, P.; van der Schoot, P.; Schenning, A. P. J. H.; Meijer, E. W. *Science* **2006**, *313*, 80−83. (b) Bouteiller, L.; van der Schoot, P. *J. Am. Chem. Soc.* **2012**, *134*, 1363−1366.
(21) Filot, I. A. W.; Palmans, A. R. A.; Hilbers, P. A. J.; Hensen, E. J. M.; de Greef, T. F. A.; Pidko, E. A. *Phys. Chem. Chem. Phys.* **2012**, *14*, 13997−14002.
(22) (a) Dill, K. A.; Bromberg, S.; Yue, K.; Chan, H. S.; Fiebig, K. M.; Yee, D. P.; Thomas, P. D.; Chan, H. S. *Protein Sci.* **1995**, *4*, 561−602. (b) Harano, Y.; Kinoshita, M. *Biophys. J.* **2005**, *89*, 2701−2710.
(23) Dunitz, J. D.; Ibberson, R. M. *Angew. Chem., Int. Ed.* **2008**, *47*, 4208−4210.
(24) Lacks, D. J. *J. Chem. Phys.* **1995**, *103*, 5085−5090.
(25) (a) O'Leary, D. J.; Rablen, P. R.; Meyer, M. P. *Angew. Chem., Int. Ed.* **2011**, *50*, 2564−2567. (b) Fong, A.; Meyer, M. P.; O'Leary, D. J. *Molecules* **2013**, *18*, 2281−2296.
(26) (a) Mislow, K.; Glass, A. W.; Hopps, H. B.; Simon, E.; Wahl, G. H., Jr. *J. Am. Chem. Soc.* **1964**, *86*, 1710−1732. (b) Mislow, K.; Graeve, R.; Gordon, A. J.; Wahl, G. H., Jr. *J. Am. Chem. Soc.* **1964**, *86*, 1733−1741.
(27) (a) Hunt, N. T.; Meech, S. R. *Chem. Phys. Lett.* **2003**, *378*, 195−201. (b) Sokoloff, J. B. *J. Chem. Phys.* **1988**, *89*, 2330−2335.